Nanoparticle-Induced Permeability of Lipid Membranes

Sergey Pogodin,[†] Marco Werner,[‡,§] Jens-Uwe Sommer,[‡,§] and Vladimir A. Baulin[†,⊥,*]

[†]Departament d'Enginyeria Quimica, Universitat Rovira i Virgili, 26 Avenida dels Paisos Catalans, 43007 Tarragona, Spain, [‡]Leibniz-Institut für Polymerforschung Dresden e.V., Hohe Strasse 6, 01069 Dresden, Germany, [§]Institute of Theoretical Physics, Technische Universität Dresden, 01069 Dresden, Germany, and [⊥]ICREA, 23 Passeig Lluis Companys, 08010 Barcelona, Spain

ABSTRACT Monte Carlo simulations using the bond fluctuation method with explicit solvent reveal the mechanism of enhanced permeability of lipid bilayers induced by the adsorption of nanoparticles with controlled hydrophobicity. Simulation results indicate an adsorption transition of nanoparticles on the bilayer in a certain range of relative degree of hydrophobicity. In this range the nanoparticles can translocate through the bilayer, reversibly destabilizing the structure of the bilayer and inducing enhanced permeability for water and small solutes. This transition is broader for amphiphilic nanoparticles.

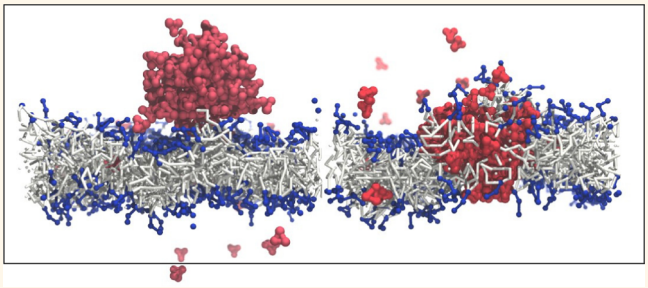

KEYWORDS: lipid bilayer · cell membrane · nanoparticles · absorption · permeability · nanotoxicity · uptake

Self-assembled lipid bilayers represent an efficient protective barrier for living cells.[1] Lipid membranes prevent passage of high molecular weight components, including nanoparticles and biopolymers inside the cells. Overcoming such barriers is a challenging problem for transmembrane drug delivery,[2] gene transfection,[3] and cell preservation.[4] Small membrane-active molecules,[5] anesthetics,[6] and neurotransmitters[7] to a certain extent can also be viewed as nanoparticles, which can interact with lipid bilayers and modify their functional properties. Apart from fundamental and practical interest, the interaction of nanoparticles with cells raises safety issues. The abundance of nanoparticles in food, food packaging, fuel, air pollution, cosmetics, and cloth puts into question the general toxicity of nanoparticles and especially their cytotoxicity, which is linked to membrane lytic ability and their ability to damage lipid membranes.[8] Despite great interest in the topic, direct microscopic information about the interaction of nanoparticles with lipid bilayers is difficult to obtain in experiments, and thus in many cases the exact mechanism of interaction or uptake of nanoparticles remains unknown.

Membrane properties and the ability to translocate through the bilayers are influenced by nanoparticle composition, size, shape, and surface properties.[9−14] In general, small solute molecules can translocate through lipid bilayers by passive diffusion,[15] while nano-objects larger than 100 nm, *e.g.*, carbon nanotubes, have difficulty passing through the bilayer by a diffusion mechanism.[5] Wise patterning may be required to reduce the energy barrier for translocation of such objects through the bilayer.[13] Nano-objects with surface patterning, striped nanoparticles, have shown enhanced translocation ability.[8]

When considering nano-objects that can translocate through membranes or that can modify the structure of lipid bilayers to allow for enhanced permeability for water and small solute molecules, one usually considers *static* structures,[9] such as pores,[16] fission and budding,[17] aggregation on the surface,[18,19] and inclusion or dissolution in the hydrophobic core of the membrane.[20,21] Recently, another *dynamic* mechanism of lipid membrane permeation by polymers was proposed.[22,23] The lipid bilayer represents a potential barrier for hydrophilic homopolymers and a potential well for hydrophobic homopolymers. It was shown that there is an intermediate range of hydrophobicity,

* Address correspondence to vladimir.baulin@urv.cat.

Received for review June 28, 2012 and accepted November 5, 2012.

Published online November 05, 2012
10.1021/nn3028858

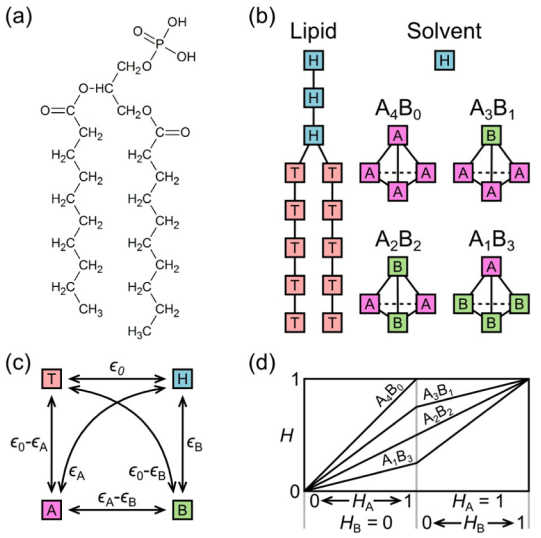

Figure 1. (a) Chemical structure of a glycerophospholipid having 10 carbon groups in each tail. (b) Models of lipid, solvent, and various nanoparticles. (c) Scheme of the interactions between the monomers of different types. (d) Average hydrophobicity of the nanoparticles *versus* the relative hydrophobicities of their A and B monomers.

when the homopolymer is close to the adsorption transition; that is, part of the time it is bound to the membrane and part of the time it is in solution. Such transition behavior destabilizes the lipid bilayer, and fluctuations in the lipid bilayer increase. This collective phenomenon leads to improved translocation of the polymer through the bilayer and significant increase of the permeability of the solvent, induced by the polymer. It is noteworthy that the resulting permeation domain on the membrane is not static and the damage to the membrane is reversible.

The objective of the present work is to show that a similar mechanism based on adsorption transition with a balanced hydrophobicity can be applied also to nanoparticles. Thus, the objective is twofold: demonstrate that (i) amphiphilic nanoparticles with controlled surface properties can translocate through lipid bilayers and (ii) the presence of such nanoparticles enhances significantly the permeability of lipid bilayers to water and small solute molecules.

RESULTS AND DISCUSSION

Different phospholipid molecules self-assemble at room temperature into bilayers that have slightly different thermodynamic properties, but usually surface area per lipid is about 60−70 Å^2 and the average volume per CH_2 group in the membrane core is 28 Å^3.[24,25] In our lattice model illustrated in Figure 1 and described in more detail in the Methods section, the lipid bilayer has an average area per lipid of $27.3a^2$, and the volume, occupied by the tails of a single lipid inside the membrane, is $91.4a^3$. Thus, we can estimate the size of the lattice site as equal to a = 1.54 Å, which is similar to the length of a carbon−carbon chemical bond, and the average bond length as about 4 Å, which is close to other estimates for the bond fluctuation method (BFM) for aliphatic chains. Then we may estimate the length of the lipid tails in the order of 10 carbon groups, which corresponds to the glycerophosphatic lipid, depicted in Figure 1a. One may notice that the thickness of the membrane core in our simulation, 10.3 Å, is slightly smaller than expected for the membrane formed by such lipids. This is due to the coarse-grained nature of our model, which reflects universal properties of the system, rather than the exact quantitative characteristics. The size of the simulation box is equal to 98.6 × 98.6 × 98.6 Å, and the effective diameters of the solvent and the nanoparticles are equal to 3.8 Å, which is comparable to the size of water molecules, and 6.1 Å, correspondingly. Nanoparticles produced in the experiment may be larger than 6.1 Å in diameter; for example, C60 is about 10 Å in diameter.[26] However one may expect similar behavior of the system as far as their size is similar to the thickness of the phospholipid membrane.

Translocations of hydrophilic nanoparticles through the bilayer occur very rarely, and, although the size of the simulated nanoparticles is only several times larger than the size of the solvent molecules, the bilayer permeability for the hydrophilic particles (H = 0) is negligible compared to the permeability of the solvent. As the hydrophobicity of the nanoparticles is increased (Figure 2), two different situations are possible. The first one takes place when the nanoparticles are able to stay dissolved in the solvent (Figure 2a). In this case their ability to penetrate through the membrane increases slowly along the increase of their average hydrophobicity, until the membrane permeability for them becomes equal to the permeability for the solvent. In our model it happens at H = 0.47 ± 0.03. Further increase of the particles' hydrophobicity leads to a faster increase of the permeability, and adsorption of the particles on the membrane surface starts to take place. Eventually, at H = 0.64 ± 0.02 the membrane becomes "quasi-transparent", in the sense that the volume fraction of the particles inside the hydrophobic membrane core, averaged over time, becomes equal to their average volume fraction in the solvent. Further increase of the hydrophobicity up to H = 0.72 reveals a maximum of the membrane permeability for the particles and a subsequent decrease of the permeability when H approaches 1.0. Figure 2a clearly shows that the maximum permeability of the membrane for the nanoparticles depends on the particle type. This is due to different "polarization" M of the particles of different types with the same average hydrophobicity H, as shown in Figure 2d. The most polar, at H = 0.72, particles of the type A_3B_1 are the most surface active; thus there is a higher tendency to be adsorbed on the membrane's surface (Figure 3a), which decreases the permeability, determined as a translocation of free

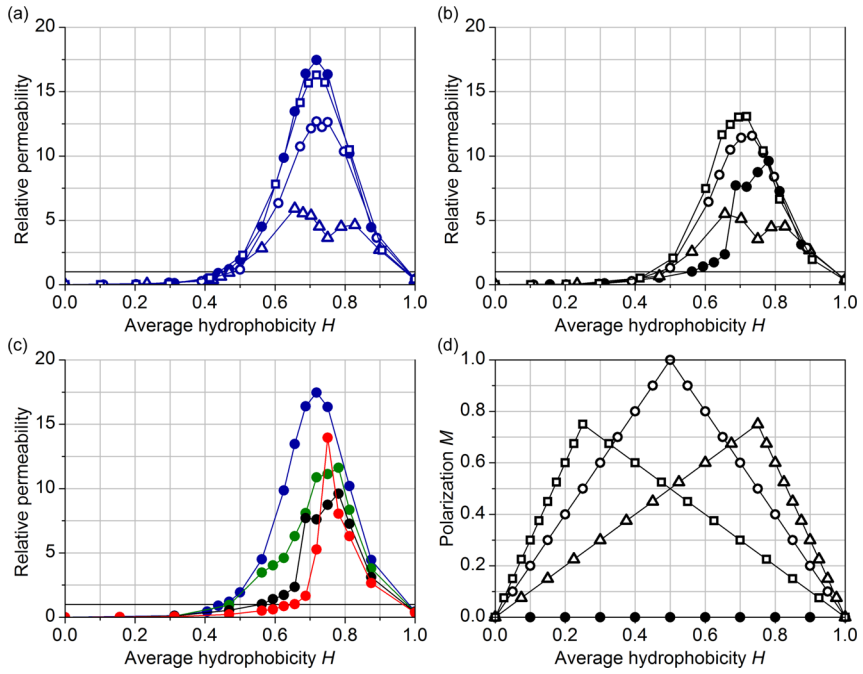

Figure 2. Relative permeability of the bilayer for nanoparticles *versus* their average hydrophobicity *H* (a−c). The amount of particles inside the simulation box is denoted by the color of the lines: 36, blue; 72, green; 144, black; 288, red. The type of particle is denoted by the shape of the symbols: A_4B_0, filled circles; A_3B_1, open triangles; A_2B_2, open circles; A_1B_3, open squares; thus the filled and the open symbols are used to better distinguish between homogeneous (A_4B_0) and amphiphilic (A_3B_1, A_2B_2, and A_1B_3) nanoparticles. The data are normalized in such a way that the permeability is equal to 1.0 (this level is shown by the plots with an additional black horizontal line), corresponding to the permeability of the membrane to the solvent in the absence of particles. The image (d) shows the dependence of the particle polarization *M* on their average hydrophobicity *H*.

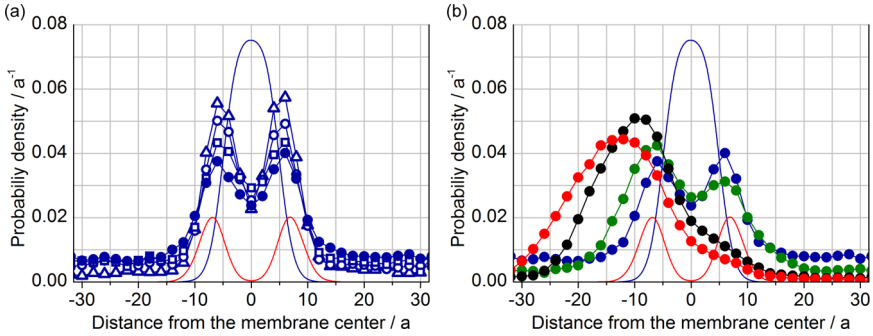

Figure 3. Probability of finding nanoparticles with average hydrophobicity $H = 0.72$ at various distances from the membrane midplane in the case of 36 particles of different type (a) or in the case of different amounts of homogeneous particles (b) (shown by the lines with symbols, designated in the same manner as in Figure 2). The red and blue lines without symbols show the position of the phospholipid tails and heads.

particles from solvent on one side of the membrane to the solvent on the other side. On the other hand the least polar amphiphilic particles A_1B_3 are less surface active, and the maximum of the permeability of the membrane for them almost coincides with that for homogeneous A_4B_0 particles.

The second scenario of the system behavior with the increase of *H* is illustrated by the snapshots in Figure 4. In our simulations, in the explored range of parameters, it was observed only for the homogeneous particles (A_4B_0) when their amount in the simulation box was 72 and larger. In this case the particles stay dissolved in the solvent (Figure 4a) up to some hydrophobicity H_{agg}, at which point they aggregate with each other (Figure 4b). This aggregation hydrophobicity was roughly estimated as 0.59, 0.40 ± 0.05, and 0.30 ± 0.05 for the cases of 72, 144, and 288 particles, correspondingly. It can be seen from Figure 2c that the hydrophobicity, at which the membrane permeability for the particles becomes equal to that for the solvent, in this case increases to the values 0.58 and 0.65 in the cases of 144 and 288 particles in the box. This happens because the large aggregate, not able to penetrate through the membrane as whole, plays the role of a local potential trap for the particles at one side of the membrane. This means that for a significant part of the time every

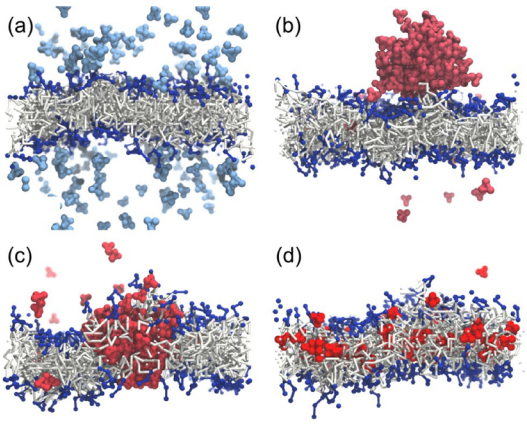

Figure 4. Typical snapshots of the system with homogeneous nanoparticles of different hydrophobicity: (a) below and (b) above the aggregation point, (c) after aggregate internalization in the membrane, and (d) after the dissolution of the aggregate in the membrane core.

particle in the box is inside the aggregate, and to translocate through the membrane it first has to escape from the aggregate and then translocate through the bilayer. This leads to an effective decrease of the membrane permeability for the particles (Figure 2). A further increase of the particles' hydrophobicity leads to the adsorption of the aggregate at the membrane surface and its further internalization (Figure 4c) inside the membrane core, with the transition happening at about $H = 0.72$. A further increase of the hydrophobicity makes the nanoparticles indistinguishable from the lipid tails, which leads to the dissolution (Figure 4d) of the aggregate inside the membrane core and to the homogeneous distribution of the particles inside the core. One may notice as well from Figure 2b,c that the aggregation of the particles shifts their permeability peak to higher values of H. This happens because when such a hydrophobic aggregate is internalized inside the hydrophobic membrane core, there appears an easier way for the particles to escape from the aggregate *via* the membrane core.

The reason the aggregation scenario was observed only for the homogeneous particles is that the amphiphilic particles of the same average hydrophobicity H have a lesser tendency to aggregate. So their aggregation hydrophobicity H_{agg} turns out to be larger than the adsorption hydrophobicity H_{ads} of the individual amphiphilic particles on the membrane surface.

The most important outcome of our simulations is the data on the influence of the nanoparticles on the membrane permeability for solvent, presented in Figure 5 and in Figure 6. It can be seen in Figure 5 that in the presence of a sufficient amount of homogeneous particles the membrane permeability for the solvent increases sharply around $H = 0.68$. This hydrophobicity corresponds to the point at which the aggregate, formed by the particles, is at the point of internalization inside the membrane. It causes significant disturbance

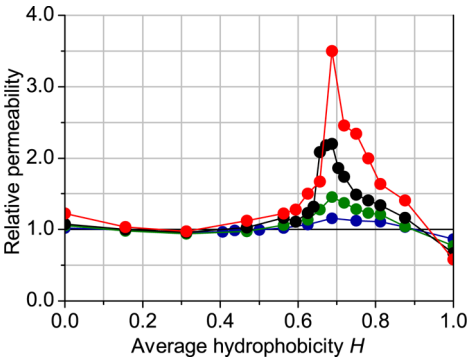

Figure 5. Relative membrane permeability for the solvent in the presence of 36, 72, 144, and 288 homogeneous nanoparticles inside the simulation box *versus* the average hydrophobicity of the particles. Coding of the lines is the same as in previous figures.

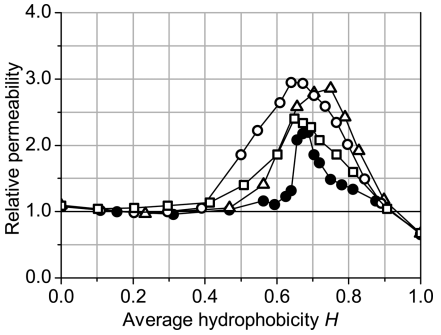

Figure 6. Relative membrane permeability for the solvent in the presence of 144 homogeneous or amphiphilic nanoparticles of different types inside the simulation box *versus* the average hydrophobicity of the particles. Coding of the lines is the same as in previous figures.

of the membrane, facilitating the solvent molecules' translocation through the bilayer in the vicinity of the aggregate (Figure 7). At higher H, the aggregate is stabilized inside the membrane core, and the membrane permeability decreases. It even becomes slightly lower than 1.0 when $H = 1$, due to the fact that the particles dissolved inside the bilayer effectively increase the thickness of the hydrophobic barrier as the solvent molecules pass through the membrane.

These findings concur with our previous results for polymer chains interacting with lipid bilayers,[22] where we have considered homopolymer chains with monomer units of relative hydrophobicity, H. Also for the case of polymers with balanced hydrophobicity of the monomer units we observe translocation events for the chain close to $H_A = 0.68$, which corresponds to the point of adsorption of the chain at the membrane's core. Also, at this point the permeability of the membrane with respect to the solvent is increased in an area close to the adsorbed chain. The fact that the relative hydrophobicity at the point of maximum translocation/permeability is larger than $H = 0.5$ is related with an insertion barrier for the chains and particles, which perturbs the self-organized phase of the lipids.

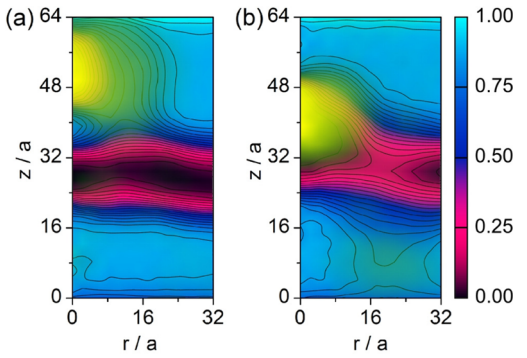

Figure 7. Typical images of the cylindrical instant distribution of the solvent (blue–pink–black gradient and equidistant level lines drawn with steps of 0.05) in the simulation box with respect to the axis of the aggregate (shown with a greenish-yellow color over the solvent distribution purple gradient and thicker level lines), formed by homogeneous nanoparticles at $H = 0.68$. In both cases all 144 particles, presented inside the simulation box, form a single large aggregate, which is (a) floating in the bulk of solvent or (b) penetrating inside the bilayer. In the last case one can see that the volume fraction of solvent inside the membrane core around the aggregate is slightly larger; thus a preferable path for solvent translocation through the bilayer is created.

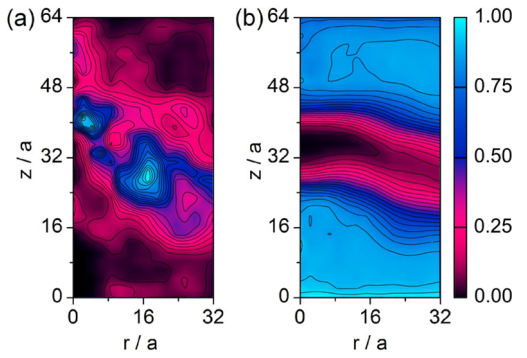

Figure 8. Typical image of the cylindrical instant distribution of (a) nanoparticles and (b) the solvent in the simulation box with respect to the center of mass of all particles presented in the system for the case of 144 nanoparticles of type A_2B_2 with relative hydrophobicity $H = 0.68$.

Despite a certain similarity between the results for polymers and nanoparticles interacting with bilayers, these objects have different sizes and structures. Due to the connectivity of the monomers into a linear chain, the polymer moves as one object, restricting the translational entropy, while nanoparticles have no internal structure and move independently. Thus, the difference between the polymers would be the size of the objects. The root mean squared radius of gyration of a chain globule studied in refs 22 and 23 with 128 monomers at $H = 0.7$ was $\sim 6.23a$ (corresponding to a diameter of $\sim$25 Å assuming a hard-sphere density distribution) and should be compared to the diameter of the nanoparticles in this work, 6.1 Å. In the case of homogeneous nanoparticles one might think that the aggregate as a whole corresponds best to a homopolymer globule in poor solvent. The absence of connectivity between the nanoparticles as well as the different geometry of the nanoparticles as compared to statistical segments of the homopolymers can lead to different reorganization dynamics close to the bilayer: so far we did not observe any adsorption–translocation–desorption event of the nanoparticle aggregates as for polymer globules.[22,23] However, longer time scales and longer polymer chains would be necessary to conclusively compare nanoparticle aggregates to polymer globules in terms of their translocation rate. We also consider amphiphilic "polar" nanoparticles, while the polymer chain discussed previously had uniform hydrophobicity. This polarization effect could be related to copolymer-like behavior. This way the nanoparticles mimic rather very short diblock copolymers.

Membrane permeability for solvent in the presence of the 144 homogeneous nanoparticles A_4B_0 is compared with the permeability in the presence of the same amount of amphiphilic particles of types A_3B_1, A_2B_2, and A_1B_3 in Figure 6. It can be seen clearly that the presence of the amphiphilic particles also increases the permeability of the membrane for solvent around $H = 0.68$, but the increase is slightly higher and, more importantly, takes place in a larger range of average hydrophobicities, compared to the case of the homogeneous particles. This can be explained by the fact that the amphiphilic nanoparticles do not form any aggregates, being individually adsorbed at the membrane surface. Thus, every adsorbed particle disturbs the membrane surface in its vicinity, increasing the local permeability for the solvent. This results in the fact that the most surface-active A_2B_2 particles (open circles in Figure 6) significantly raise the membrane permeability in the largest range of their average hydrophobicity H, while they are quite homogeneously distributed around the membrane surface and there is no place on the membrane with a content of the solvent much higher than in the rest of the bilayer (Figure 8).

CONCLUSIONS

The interaction of amphiphilic nanoparticles with controlled hydrophobicity and lipid bilayers is studied using the bond fluctuation method. Translocation of nanoparticles and permeability of the lipid bilayer for small solute molecules have been studied for different levels of relative hydrophobicity of nanoparticles. Hydrophilic nanoparticles do not translocate, and the change in the permeability of the lipid bilayer for solvent due to the presence of nanoparticles is negligible. Hydrophobic particles aggregate in clusters. These aggregates incorporate and dissolve into the hydrophobic core of the bilayer, which represents a deep potential well preventing translocation. The corresponding permeability of solvent is also small. However, there is a narrow range of relative hydrophobicity where the nanoparticles exhibit adsorption–desorption transition,

characterized by significantly increased events of translocation through the bilayer and enhanced permeability of solvent, while the associated damage to the bilayer is reversible.

In the case of amphiphilic nanoparticles, composed of hydrophobic and hydrophilic units, the region of membrane activity inducing a higher solvent permeability is broader. Thus, the use of amphiphilic nanoparticles may be preferable in some applications, since it requires less precision in identifying the transition point. In addition, amphiphilic particles do not aggregate in solution; thus, they are potentially less toxic and more soluble.

METHODS

The universality of self-assembled structures[27] formed by lipids and short block copolymers allows using coarse graining models for the description of collective phenomena in lipid bilayers.[28] Elimination of some chemical details and a reduced number of degrees of freedom in coarse-grained models speed up computation significantly, but still capture qualitative features of self-assembled structures and incorporate essential physics.[27]

The bond fluctuation method[29,30] with explicit solvent[31] is used to model self-assembled bilayers of lipids and their interactions with nanoparticles. This is a well-established and widely used theoretical method used to simulate various polymer systems[29−35] and lipid bilayers.[22,23,36,37] It was shown that the BFM accurately reproduces proper dynamical behavior of dense polymer systems, polymer solutions, networks, copolymers, and dendrimers. Muller *et al.*[36,37] have shown that the BFM model can reproduce essential properties of lipid bilayers and can address essential properties such as membrane fusion and pore nucleation. We use the same model for lipid bilayers, which was employed earlier to study the interaction between a polymer chain and a lipid bilayer.[22,23] Within this model each lipid molecule is represented by 3 hydrophilic (H) and 10 hydrophobic (T) cubic monomers, joined with each other (Figure 1b) and placed on a periodic cubic lattice of size $64a \times 64a \times 64a$, periodic in *xy*-directions, where *a* is the lattice size. The length of the bonds between the monomers may fluctuate in the range $[2a...10^{1/2}a]$. Explicit solvent molecules, represented by individual H-monomers, fill in the free space on the lattice with a volume fraction 0.5, which corresponds to a dense system in the framework of the BFM.[31] The interaction parameter $\varepsilon_0 = 0.8kT$ (Figure 1c) ensures a penalty for the contacts between the H- and the T-monomers, thus forcing the self-assembly of the phospholipids in the bilayer structure. Under such conditions approximately 300 lipids are necessary to form an equilibrated membrane parallel to the *xy*-facet of the simulation box.[22,23] When the lipids are preordered in a rough bilayer structure in the middle of the simulation box in the initial state, the sufficient relaxation time is about 1 million Monte Carlo (MC) steps, so we did every simulation run 100 million MC steps long, which took about 2 cpu-days.

We consider four types of nanoparticles (A_4B_0, A_3B_1, A_2B_2, and A_1B_3), representing different levels of hydrophobicity of nanoparticles. They are simulated as small tetrahedrons, composed of monomers of two kinds, A and B (Figure 1b). The interactions between A-, B-, T-, and H-monomers (Figure 1c) depend on two additional parameters, ε_A and ε_B. They are grouped into relative hydrophobicities, H_A and H_B, according to

$$H_A = \frac{\varepsilon_A}{\varepsilon_0}, \quad H_B = \frac{\varepsilon_B}{\varepsilon_0}, \quad 0 \le H_B \le H_A \le 1 \qquad (1)$$

Hence, if $H_A = 0$, A-monomers are hydrophilic and not distinguishable from H-monomers, while if $H_A = 1$, they are hydrophobic and identical to T-monomers. The intermediate values of H_A correspond to intermediate hydrophobicity. The same notation is used for H_B and B-monomers.

The nanoparticles can also be characterized by the average relative hydrophobicity, *H*, and by the "polarization", *M*, determined for the particles of type A_iB_j by

$$H = \frac{i}{4}H_A + \frac{j}{4}H_B, \quad M = \frac{i}{2}(H_A - H) - \frac{j}{2}(H_B - H),$$
$$0 \le H, M \le 1 \qquad (2)$$

To maintain an unambiguous correspondence among *H*, H_A, and H_B for nanoparticles of all types, we changed these parameters according to the procedure shown in Figure 1d. To change the average hydrophobicity *H* of the particles from 0 to 1, we first increase H_A from 0 to 1, at fixed $H_B = 0$, thus reaching a maximum "polarization" of the amphiphilic particles at $H_A = 1$ and $H_B = 0$; then we increase H_B from 0 to 1, at the fixed $H_A = 1$.

The results are obtained in a series of simulations with 36 and 144 nanoparticles in the simulation box. For homogeneous nanoparticles (A_4B_0) additional calculations with 72 and 288 particles were performed. To compare the lipid membrane permeability for nanoparticles with the permeability for the solvent, we determine the permeability of the membrane for the molecules of the specified type α as

$$P_\alpha = \frac{n_\alpha}{N_\alpha \Delta t} \qquad (3)$$

where N_α is the total amount of the α molecules inside the simulation box and n_α is the number of translocation events of such molecules through the bilayer during the time interval Δt.

The counting of the translocation events was performed in a way slightly different from the one used in ref 22 in order to be more accurate when the membrane is bent. Instead of calculation of the membrane position and the boundaries *via* averaging over the whole simulation box, the local boundaries of the bilayer were calculated and used in the present work to determine the translocation events, as follows: the *xy*-facet of the simulation box was divided into regions of size 8×8, and the local positions of the bilayer center were calculated as $\bar{z} = \langle z \rangle$, where the averaging was performed over all lipid monomers in the given region. Also the total amount of lipid monomers in every region and the full thickness of the membrane $2\sigma_z$ were calculated ($\sigma_z^2 = \langle z^2 \rangle - \bar{z}^2$). Then the regions where the amount of lipid monomers was less than 30% of average were marked as occupied by "pores", while the rest of the regions were used to determine the average full thickness of the membrane $2\bar{\sigma}_z$. Finally, the center z_{xy} of the membrane at the point (*x*,*y*) was approximated by the linear interpolation between the closest "nonpore" regions, and the membrane boundaries at that point were approximated as $z_{xy\pm} = z_{xy} \pm \bar{\sigma}_z$ for calculations of the solvent permeability, and as $z_{xy\pm} = z_{xy} \pm 3\bar{\sigma}_z$ for calculations of the nanoparticle permeability. Larger boundaries of the membrane for the calculations of its permeability for the nanoparticles are necessary because, in the case of fully hydrophobic particles, such particles are entrapped inside the membrane core, and, oscillating inside such a potential well, they are able to trespass the boundaries intensively when the boundaries are too narrow, thus producing a huge result for permeability, which should be considered as an artifact of the calculations. On the other hand, too wide boundaries of the membrane, when used for the calculations of the membrane permeability for solvent, may unnecessarily exclude some events of the solvent molecules' translocation through the bilayer, thus suppressing the measured values of the permeability. Note also that the shapes of nanoparticle aggregates are fluctuating, and although artifacts as described above can be reduced efficiently using a good compromise for the thresholds $z_{xy\pm}$, they cannot be completely excluded.

Conflict of Interest: The authors declare no competing financial interest.

Acknowledgment. We gratefully acknowledge the Leibniz-Society (SAW Grant) for financial support and acknowledge the

Center for High Performance Computing at the Technische Universität Dresden and the Universitat Rovira i Virgili for computing time and technical support.

REFERENCES AND NOTES

1. Alberts, B.; Johnson, A.; Lewis, J.; Raff, M.; Roberts, K.; Walter, P. *Molecular Biology of the Cell*, 5th ed.; Garland Science: New York, 2008.
2. Moghimi, S. M.; Hunter, A. C.; Murray, J. C. Nanomedicine: Current Status and Future Prospects. *FASEB J.* **2005**, *19*, 311–330.
3. Sitharaman, B.; Zakharian, T. Y.; Saraf, A.; Misra, P.; Ashcroft, J.; Pan, S.; Pham, Q. P.; Mikos, A. G.; Wilson, L. J.; Engler, D. A. Water-Soluble Fullerene (C60) Derivatives as Nonviral Gene-Delivery Vectors. *Mol. Pharmaceutics* **2008**, *5*, 567–578.
4. Scott, K. L.; Lecak, J.; Acker, J. Biopreservation of Red Blood Cells: Past, Present, and Future. *Transfus. Med. Rev.* **2005**, *19*, 127.
5. Dawson, K. A.; Salvati, A.; Lynch, I. Nanoparticles Reconstruct Lipids. *Nat. Nanotechnol.* **2009**, *4*, 84–85.
6. Tu, K.; Tarek, M.; Klein, M. L.; Scharf, D. Effects of Anesthetics on the Structure of a Phospholipid Bilayer: Molecular-Dynamics Investigation of Halothane in the Hydrated Liquid Crystal Phase of Dipalmitoylphosphatidylcholine. *Biophys. J.* **1998**, *75*, 2123–2134.
7. Seeger, H. M.; Gudmundsson, M. L.; Heimburg, T. How Anesthetics, Neurotransmitters, and Antibiotics Influence the Relaxation Processes in Lipid Membranes. *J. Phys. Chem. B* **2007**, *111*, 13858–13866.
8. Verma, A.; Uzun, O.; Hu, Y.; Hu, Y.; Han, H.-S.; Watson, S.; Chen, N.; Irvine, D. J.; Stellacci, F. Surface-Structure-Regulated Cell-Membrane Penetration by Monolayer-Protected Nanoparticles. *Nat. Mater.* **2008**, *7*, 588–595.
9. Schulz, M.; Olubummo, A.; Binder, W. H. Beyond the Lipid-Bilayer: Interaction of Polymers and Nanoparticles with Membranes. *Soft Matter* **2012**, *8*, 4849–4864.
10. Ding, H.-M.; Ma, Y.-Q. Interaction Between Janus Particles and Membranes. *Nanoscale* **2012**, *4*, 1116–1122.
11. Ding, H.-M.; Tian, W.-D.; Ma, Y.-Q. Designing Nanoparticle Translocation through Membranes by Computer Simulations. *ACS Nano* **2012**, *6*, 1230–1238.
12. Van Lehn, R. C.; Alexander-Katz, A. Penetration of Lipid Bilayers by Nanoparticles with Environmentally-Responsive Surfaces: Simulation and Theory. *Soft Matter* **2011**, *7*, 11392–11404.
13. Pogodin, S.; Slater, N. K. H.; Baulin, V. A. Surface Patterning of Carbon Nanotubes Can Enhance Their Penetration through a Phospholipid Bilayer. *ACS Nano* **2011**, *5*, 1141–1146.
14. Pogodin, S.; Slater, N. K. H.; Baulin, V. A. Biomolecule Surface Patterning May Enhance Membrane Association. *ACS Nano* **2012**, *6*, 1308–1313.
15. Orsi, M.; Essex, J. W. Permeability of Drugs and Hormones Through a Lipid Bilayer: Insights from Dual-Resolution Molecular Dynamics. *Soft Matter* **2010**, *6*, 3797–3808.
16. Jenssen, H.; Hamill, P.; Hancock, R. E. W. Peptide Antimicrobial Agents. *Clin. Microbiol. Rev.* **2006**, *19*, 491–511.
17. Noguchi, H.; Takasu, M. Adhesion of Nanoparticles to Vesicles: A Brownian Dynamics Simulation. *Biophys. J.* **2002**, *83*, 299–308.
18. Saric, A.; Cacciuto, A. Fluid Membranes Can Drive Linear Aggregation of Adsorbed Spherical Nanoparticles. *Phys. Rev. Lett.* **2012**, *108*, 118101.
19. Li, Y.; Chen, X.; Gu, N. Computational Investigation of Interaction between Nanoparticles and Membranes: Hydrophobic/Hydrophilic Effect. *J. Phys. Chem. B* **2008**, *112*.
20. Wong-Ekkabut, J.; Baoukina, S.; Triampo, W.; Tang, I.-M.; Tieleman, D. P.; Monticelli, L. Computer Simulation Study of Fullerene Translocation through Lipid Membranes. *Nat. Nanotechnol.* **2008**, *3*, 363–368.
21. Jusufi, A.; DeVane, R. H.; Shinoda, W.; Klein, M. Nanoscale Carbon Particles and the Stability of Lipid Bilayers. *Soft Matter* **2011**, *7*, 1139–1146.
22. Sommer, J.-U.; Werner, M.; Baulin, V. A. Critical Adsorption Controls Translocation of Polymer Chain through Lipid Bilayers and Permeation of Solvent. *Europhys. Lett.* **2012**, *98*, 18003.
23. Werner, M.; Sommer, J.-U.; Baulin, V. A. Homo-Polymers with Balanced Hydrophobicity Translocate through Lipid Bilayers and Enhance Local Solvent Permeability. *Soft Matter* **2012**, *8*, 11714.
24. Nagle, J. F.; Tristram-Nagle, S. Structure of Lipid Bilayers. *Biochim. Biophys. Acta* **2000**, *1469*, 159–195.
25. Mathai, J. C.; Tristram-Nagle, S.; Nagle, J. F.; Zeidel, M. Structural Determinants of Water Permeability through the Lipid Membrane. *J. Gen. Physiol.* **2008**, *131*, 69–76.
26. Goel, A.; Howard, J. B.; Sande, J. B. V. Size Analysis of Single Fullerene Molecules by Electron Microscopy. *Carbon* **2004**, *42*, 1907–1915.
27. Muller, M.; Katsov, K.; Schick, M. Biological and Synthetic Membranes: What Can Be Learned from a Coarse-Grained Description?. *Phys. Rep.* **2006**, *434*, 113–176.
28. Muller, M.; Katsov, K.; Schick, M. Coarse-Grained Models and Collective Phenomena in Membranes: Computer Simulation of Membrane Fusion. *J. Polym. Sci. B: Polym. Phys.* **2003**, *41*.
29. Carmesin, I.; Kremer, K. The Bond Fluctuation Method: a New Effective Algorithm for the Dynamics of Polymers in All Spatial Dimensions. *Macromolecules* **1988**, *21*, 2819–2823.
30. Deutsch, H.; Binder, K. Interdiffusion and Self-Diffusion in Polymer Mixtures: A Monte Carlo Study. *J. Chem. Phys.* **1991**, *94*, 2294–2304.
31. Werner, M.; Sommer, J.-U. Polymer-Decorated Tethered Membranes under Good- and Poor-Solvent Conditions. *Eur. Phys. J. E* **2010**, *31*, 383–392.
32. Molina-Mateo, J.; Salmerón Sánchez, M.; Monleón Pradas, M.; Torregrosa Cabanilles, C. Multilayer Adsorption by Monte Carlo Simulation. *Phys. A* **2012**, *391*, 4774–4782.
33. Pandav, G.; Pryamitsyn, V.; Gallow, K. C.; Loo, J.; Genzer, Y.-L.; Ganesan, V. Phase Behavior of Gradient Copolymer Solutions: a Monte Carlo SimulationStudy. *Soft Matter* **2012**, *8*, 6471–6482.
34. Lange, F.; Schwenke, K.; Kurakazu, M.; Akagi, Y.; Chung, U.-i.; Lang, M.; Sommer, J.-U.; Sakai, T.; Saalwachter, K. Connectivity and Structural Defects in Model Hydrogels: A Combined Proton NMR and Monte Carlo Simulation Study. *Macromolecules* **2011**, *44*, 9666–9674.
35. Ivanov, V. A.; Rodionova, A. S.; An, E. A.; Martemyanova, M. R.; Stukan, J. A.; Müller, M.; Paul, W.; Binder, K. Orientational Ordering Transitions of Semiflexible Polymers in Thin Films: A Monte Carlo Simulation. *Phys. Rev. E* **2011**, *84*, 041810.
36. Muller, M.; Katsov, K.; Schick, M. A New Mechanism of Model Membrane Fusion Determined from Monte Carlo Simulation. *Biophys. J.* **2003**, *85*, 1611–1623.
37. Muller, M.; Schick, M. Structure and Nucleation of Pores in Polymeric Bilayers: A Monte Carlo Simulation. *J. Chem. Phys.* **1996**, *105*, 8282–8292.